Facilely cross-linking polybenzimidazole with polycarboxylic acids to improve H_2/CO_2 separation performance

Leiqing Hu[1], Vinh T. Bui[1], Liang Huang[1], Rajinder P. Singh[2], Haiqing Lin[1*]

[1]Department of Chemical and Biological Engineering, University at Buffalo, The State University of New York, Buffalo, NY 14260, USA

[2]Materials Physics and Applications Division, Carbon Capture and Separations for Energy Applications (CaSEA) Labs, Los Alamos National Laboratory, Los Alamos, NM 87545, USA

*Corresponding author, E-mail: haiqingl@buffalo.edu

ABSTRACT

Polybenzimidazole (PBI) with a strong size-sieving ability exhibits attractive H_2/CO_2 separation properties for blue H_2 production and CO_2 capture. Herein we report that PBI can be facilely cross-linked with polycarboxylic acids, oxalic acid (OA) and trans-aconitic acid (TaA), to improve its separation performance. The acids react with the amines on the PBI chains, decreasing free volume and increasing size-sieving ability. The acid doping increases H_2/CO_2 selectivity from 12 to as high as 45 at 35 ℃. The acid-doped samples demonstrate stable H_2/CO_2 separation performance when challenged with simulated syngas containing water vapor at 150 ℃, which surpasses state-of-the-art polymers and Robeson's upper bound for H_2/CO_2 separation.

Keywords: polybenzimidazole; polycarboxylic acid; H_2/CO_2 separation; cross-linking; membranes; carbon capture

1. INTRODUCTION

Pre-combustion CO_2 capture with H_2 production is a promising approach to eliminate the emission of CO_2 from large source points such as power plants, realizing a clean utilization of fossil fuels.[1-5] In this process, fuels are gasified to generate gas mixtures containing H_2 and CO, and the CO is further shifted to H_2 and CO_2.[6] For H_2 to be used in a green manner, the CO_2 must be captured for utilization or sequestered. Membrane technology has been extensively explored for H_2/CO_2 separation application due to its inherently high energy efficiency, small footprint, easy scale-up and low maintenance.[4, 7-10]

Gas transport through nonporous polymers usually follows the solution-diffusion mechanism, and gas permeability (P_A) can be expressed as:[9]

$$P_A = S_A \times D_A \quad (1)$$

where S_A is gas solubility, and D_A is diffusion coefficient. Gas selectivity ($\alpha_{A/B}$) is the ratio of their permeability (i.e., $\alpha_{A/B} = P_A/P_B$) and the combination of solubility selectivity (S_A/S_B) and diffusivity selectivity (D_A/D_B). For H_2/CO_2 separation, the S_A/S_B is always less than 1 because H_2 is less condensable than CO_2.[8] On the other hand, H_2 has a smaller molecular size (2.89 Å) than CO_2 (3.3 Å); therefore, membrane materials with a strong size-sieving ability is desirable to achieve high diffusivity selectivity, and thus high permeability selectivity.[8]

Industrial gas separation membranes are usually made of polymers, and polybenzimidazole (PBI) with a glass transition temperature of above 400 °C has emerged as a leading polymer for H_2/CO_2 separation at high temperatures.[8, 11-13] Commercial *m*-PBI exhibited H_2 permeability of 27 Barrer (1 Barrer = 10^{-10} cm^3 (STP) cm^{-2} s^{-1} $cmHg^{-1}$) and H_2/CO_2 selectivity of 16 at 150 °C.[4] PBI

was further cross-linked with terephthaloyl chloride (TCL),[7] 1,3,5-tris(bromomethyl)benzene (TBB),[14] and α,α'-dibromo-p-xylene (DBX)[15] to enhance the size-sieving ability and thus H_2/CO_2 selectivity. For example, the cross-linking with TCL increased H_2/CO_2 selectivity by almost 100% and retained 78% H_2 permeability at 150 °C.[7] For optimal performance, the cross-linkers should have multi-functional groups with high reactivity with PBI and low molecular weight to retain the PBI structure.[16]

Recently, we reported a facile cross-linking of PBI via proton transfer and hydrogen bonding using phosphoric acid (H_3PO_4) and sulfuric acid (H_2SO_4).[4] Increasing the acid doping level (defined as the molar ratio of the acid to PBI repeating units) resulted in a phenomenal increase in H_2/CO_2 selectivity.[4] For instance, as the doping level approached 1, H_2/CO_2 selectivity reached an unprecedented value of 140 at 150 °C. H_3PO_4 has pK_{a1}, pK_{a2}, and pK_{a3} values of 2.15, 7.20, and 12.3, respectively, suggesting that it has only one free proton. By contrast, H_2SO_4 has two free protons (<1 for pK_{a1} and 1.92 for pK_{a2}) and stronger acidity than H_3PO_4. Interestingly, at a doping level of ≈ 0.24, H_2SO_4 and H_3PO_4 showed very similar H_2/CO_2 separation properties, despite their difference in the free protons and pK_a values.[4] Therefore, the understanding the effect of the number of free protons and acidity strength on the H_2/CO_2 separation properties can be critical to designing high-performance membrane materials for this separation.

Herein we chose two polycarboxylic acids for PBI doping, namely oxalic acid (OA) and trans-aconitic acid (TaA), as shown in Fig. 1a,b. OA has two free protons with pK_{a1} and pK_{a2} values of 1.27 and 4.27, respectively,[17] and TaA has three protons with pK_{a1}, pK_{a2}, and pK_{a3} values of 2.91, 4.33, and 6.16, respectively.[18] Both acids have similar structures and stronger

acidity than H_3PO_4. We systematically determine the effect of the acid doping on physical properties of PBI (such as density, thermal stability, and free volume) and gas transport properties (such as pure-gas sorption and pure- and mixed-gas permeability) at various temperatures. The samples with promising separation properties were further evaluated with simulated wet syngas mixtures for extended tests to demonstrate their promise for industrial H_2/CO_2 separation.

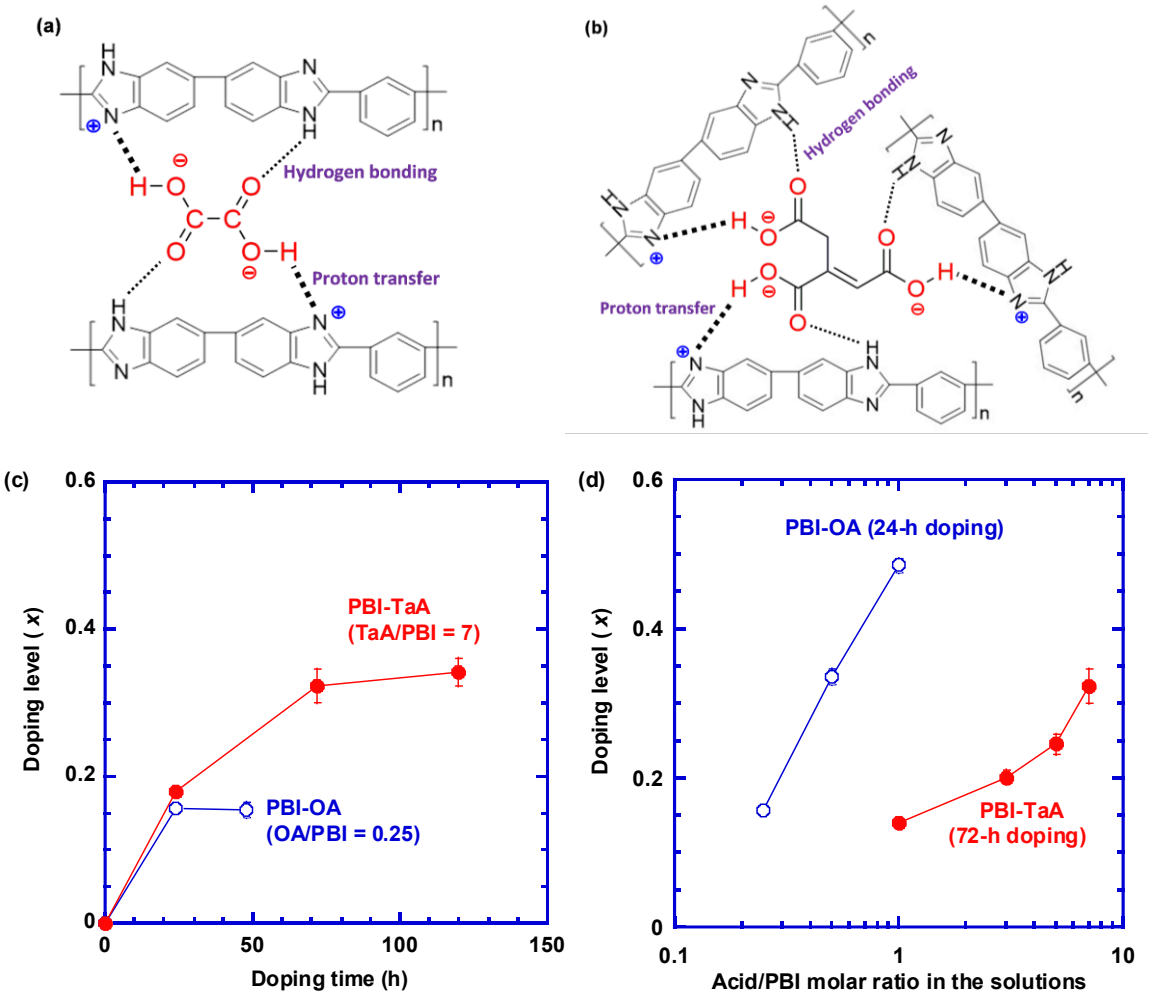

Fig. 1. Cross-linking PBI by OA and TaA. Schematic illustration of (a) PBI-OA and (b) PBI-TaA. (c) Doping level as a function of the doping time. The molar ratio of the acid in the solution to the PBI repeating unit is 0.25 for OA and 7 for TaA. (d) Effect of the acid/PBI molar ratio in the doping solutions on the doping level at equilibrium.

2. EXPERIMENTAL SECTION

2.1 Materials

Celazole® PBI S10 solution was purchased from PBI Performance Products Inc. (Charlotte, NC). The solution contains ≈ 9.5 wt% PBI (with a molecular weight of 35 kDa) in N,N-dimethylacetamide (DMAc). OA, TaA, and methanol were procured from Sigma-Aldrich Corporation (St. Louis, MO). Gas cylinders of H_2, CO_2, and N_2 with ultrahigh purity were obtained from Airgas Inc. (Buffalo, NY).

2.2 Preparation of thin films

PBI films were prepared by a solution casting method.[4, 7] First, ~2 mL of PBI S10 solution was filtered through a 0.45 μm syringe filter (Thermo Fisher Scientific, Waltham, MA). Second, the filtered solution was cast on a glass plate using a casting knife (BYK-Gardner, Pompano Beach, FL). Third, the liquid film was dried overnight in a conventional oven at 60 ℃ under N_2 flow, followed by heating at 200 ℃ under vacuum for 48 h. Fourth, the dried film was peeled off the plate and then immersed in methanol at ≈ 23 ℃ for 24 h to remove the residual DMAc. Finally, the film was vacuum-dried at 100 ℃ for 12 h. The PBI film was determined to have a thickness of ≈ 12 μm.

To prepare an acid-doped film, a PBI film (~ 120 mg) was first immersed in 100 mL methanol at ≈ 23 ℃. Second, the desired amount of OA or TaA was added to the solution. The molar ratio of the acid in the solutions to the repeating units of the PBI film was varied from 0.25 to 1 for OA, and from 1 to 7 for TaA to achieve different doping levels. Doping time was set at 24 h for OA and 72 h for TaA to ensure that the acid was evenly distributed in the film at equilibrium.

Finally, the film was taken out of the solution and dried in the vacuum oven at 100 ℃ for 12 h. The doping level (x) was calculated using the following equation:

$$x = \frac{\Delta m / M_a}{m_0 / M_p} \tag{2}$$

where M_a is the molar mass of the acid (90 g mol^{-1} for OA and 174 g mol^{-1} for TaA), and M_p is the molar mass of the PBI repeating unit (308 g mol^{-1}). The m_0 is the mass of the dry sample before the acid doping, and Δm is the mass increase caused by the acid doping. The doped samples are denoted as PBI-OA$_x$ or PBI-TaA$_x$, depending on the acid used.

2.3 Characterization of PBI-OA and PBI-TaA films

Attenuated total reflection—Fourier transform infrared spectroscopy (ATR-FTIR) was performed using a vertex 70 Burker spectrometer (Bruker Scientific LLC, Billerica, MA). For each sample, 100 scans were performed in the range of 450-4000 cm^{-1} at 4 cm^{-1} resolution. Thermal properties of the samples were determined using an SDT Q600 thermogravimetric analyzer (TA Instruments, New Castle, DE) from ≈ 23 ℃ to 800 ℃ at a ramping rate of 10 ℃/min under N_2 flow. The ramping rate of 10 ℃/min is typical for the study of polymers, as used in other reports.[4, 7, 14, 19]

Wide-angle X-ray diffraction (WAXD) patterns were obtained using a Rigaku Ultima IV X-ray diffractometer (Rigaku Analytical Devices, Wilmington, MA) with the CuKα x-ray wavelength of 1.54 Å. The scanning has a 2θ range of 5 – 45° and a rate of 1.0 °/min.

The sample density (ρ_M) was determined using an analytical balance (Mettler-Toledo, Columbus, OH) based on the Archimedes' principle. The ρ_M can be calculated as followed:[4, 7]

$$\rho_M = \frac{m_A}{m_A - m_L}\rho_L \quad (3)$$

where m_A and m_L are the sample mass in air and an auxiliary liquid, respectively. ρ_L is the density of the auxiliary liquid (i.e., iso-octane with a density of 0.69 g/cm^3).

Pure-gas permeability was determined at various pressures and temperatures via a constant-volume and variable-pressure system. The permeability was calculated using the following equation:[4, 7]

$$P_A = \frac{V_p \cdot l_m}{p_2 A_m RT}\left[\left(\frac{dp_1}{dt}\right)_{ss} - \left(\frac{dp_1}{dt}\right)_{leak}\right] \quad (4)$$

where V_p is the downstream volume, l_m is the film thickness, A_m is the effective film area for gas transport, R is the gas constant, and T is the temperature. The $(dp_1/dt)_{ss}$ and $(dp_1/dt)_{leak}$ are the steady-state rate of pressure rise in the downstream volume at the feed pressure (p_2) and under vacuum, respectively.

Mixed-gas permeability was determined using a constant-pressure and variable-volume apparatus with a sweep gas of N_2 on the permeate side and can be calculated using Eq. (5):[4, 7]

$$P_A = \frac{x_A \cdot Q_S \cdot l_m}{x_{sweep} \cdot A_m (p_{2,A} - p_{1,A})} \quad (5)$$

where Q_S is the flow rate of the sweep gas. The x_A and x_{sweep} are the mole fraction of gas component A and sweep gas in the sweep-out stream, respectively, which were measured using a 3000 Micro GC (Inficon Inc., Syracuse, NY). For the long-term stability testing, water vapor was introduced by flowing the feed gas through a water bubbler at 23 °C before entering the permeation cell. Since the permeation cell was at 150 °C, water condensation in the cell was not expected.

Gas sorption isotherms of the samples (~ 80 mg) with a thickness of ≈12 μm were determined using a gravimetric sorption analyzer of IGA 001 (Hiden Isochema, Warrington, UK), at various pressures (i.e., 3.4 bar, 7.0 bar, and 10 bar) and temperatures (i.e., 35 ℃ and 150 ℃). CO_2 and C_2H_6 sorption at each pressure reached equilibrium in ~ 10 h and ~ 20 h, respectively. The buoyancy effect was considered in the calculation of gas sorption.[4, 7]

3. RESULTS AND DISCUSSION

3.1 Effect of acid doping on physical properties

Fig. 1c displays the effect of the doping time on the acid doping level of ≈ 12 μm thin PBI films. The doping level increases with increasing doping time and levels off after 24 h for PBI-OA and 72 h for PBI-TaA. The difference is consistent as TaA has a larger molecular size than OA, and thus requires a longer doping time before reaching equilibrium. Therefore, the doping time was set at 24 h for PBI-OA and 72 h for PBI-TaA to ensure even acid distribution in the films. Fig. 1d elucidates the method used to control the doping level of PBI films (i.e., changing the molar ratio of the acid to the PBI repeating units in the doping solutions). Increasing the acid amount increases the doping level. Due to the equilibrium for the acids between the solution and the PBI films, the doping level is lower than the molar ratio of the acid to the PBI repeating units in the solutions, particularly at high doping levels. Therefore, the maximal doping level obtained in this study was 0.32 for TaA and 0.49 for OA.

Fig. 2a displays the FTIR spectra of both PBI-$OA_{0.49}$ and PBI-$TaA_{0.32}$, which exhibit a characteristic peak of COO^- at 1550 cm^{-1}.[20] This suggests that the protons transfer from the

carboxylic acid (-COOH) groups to the amine groups on the PBI chains, thus confirming the acid-base reaction. PBI-TaA$_{0.32}$ shows a small characteristic peak of the unreacted -COOH groups at 1720 cm^{-1}, presumably due to the high pKa$_3$ value and low acidity. The C=N stretching can be seen on PBI spectra at 1620 cm^{-1} but shifts to 1630 cm^{-1} for the acid-doped samples because of the hydrogen bonding.[21, 22] The N-H stretching of the imidazole rings on the PBI chains overlaps with the hydrogen bonding between the PBI and acid, and thus are not displayed in Fig. 2a.[14]

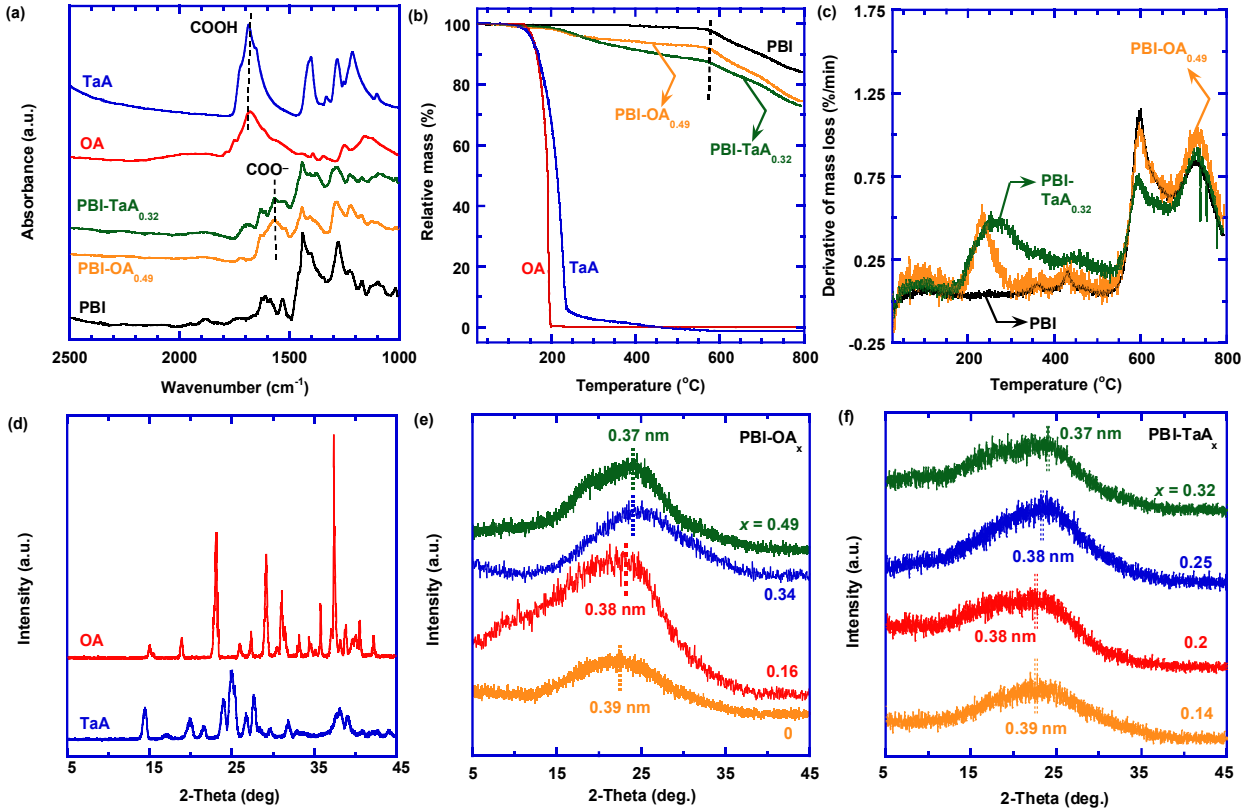

Fig. 2. Characterization of PBI, OA, TaA, PBI-OA$_{0.49}$, and PBI-TaA$_{0.32}$. (a) FTIR spectra; (b) TGA curves; (c) derivative thermogravimetric analysis (DTA) curves; WAXD patterns of (d) pure OA and TaA, (e) PBI-OA$_x$, and (f) PBI-TaA$_x$. The double dotted lines show the peaks and corresponding 2θ values, which are used to calculate the *d*-spacing.

Fig. 2b,c compares the thermal stability of pure acids and two representative samples of PBI-OA and PBI-TaA. Both OA and TaA start to degrade at ~150 °C. However, PBI-$OA_{0.49}$ and PBI-$TaA_{0.32}$ have degradation temperatures of ~230 °C and ~260 °C, respectively, indicating improved acid thermal stability when reacted with PBI. At 580 °C, PBI exhibits 2% mass loss, while PBI-$OA_{0.49}$ containing 12 wt% OA and PBI-$TaA_{0.32}$ containing 15 wt% TaA show a mass loss of 8.5 wt% and 13 wt%, respectively. The lower mass loss values than the acid content can be ascribed to the partial degradation of the acids. The DTA peaks above 580 °C are attributed to the degradation of the PBI backbones.[7]

Fig. 2d displays WAXD patterns of pure OA and TaA at ≈ 23 °C, and the sharp peaks indicate that they are crystalline. By contrast, these sharp peaks disappear in the patterns of the acid-doped PBIs (cf. Fig. 2e,f), suggesting that the reaction with PBI causes structure modification of the acids, from crystalline to amorphous in PBI films. PBI has a characteristic peak at 22.5°, corresponding to a *d*-spacing (represents the average inter-segmental distance between polymer chains) of 0.39 nm according to Bragg's equation.[23] By contrast, PBI-$OA_{0.49}$ and PBI-$TaA_{0.32}$ show the *d*-spacing of 0.37 nm, confirming the tightened structure by acid doping. Fig. S1 shows that increasing temperature increases the *d*-spacing.

Fig. S2a shows that the density of the acid-doped PBI (ρ_m) increases with increasing acid doping level. To elucidate the reaction between the acids and PBI, the ρ_m is described using an additive model:[24]

$$\frac{1}{\rho_m} = \frac{\omega_p}{\rho_p} + \frac{\omega_a}{\rho_a} = \frac{1}{\rho_p} + \left(\frac{1}{\rho_a} - \frac{1}{\rho_p} \right) \omega_a \tag{6}$$

where ω is the weight fraction, and the subscripts of p and a represent the PBI and amorphous acid, respectively. This model assumes that the density of PBI and amorphous acid are independent of the composition. While this model might not depict the physical presentation of the acid-doped PBI, there is no reported way to obtain the ρ_P and ρ_a values, which are also needed for the analysis of the free volume. Fig. 3a also shows that the ρ_m data can be satisfactorily modeled with the ρ_a value of 2.27 g/cm^3 for OA and 1.87 g/cm^3 for TaA, which are higher than the pure acid densities (1.90 g/cm^3 for OA and 1.70 g/cm^3 for TaA), though the pure acids are crystalline. While the crystalline phase of most materials exhibits higher density than their amorphous phase, several polymers were reported with higher density for the amorphous phase than the crystalline phase, such as poly(4-methyl-1-pentene) (PMP)[25] and poly(2,6-dimethyl-1,4-phenylene)oxide (PPO).[26] Nevertheless, the preparation of amorphous acids and their density measurement is beyond the scope of this study.

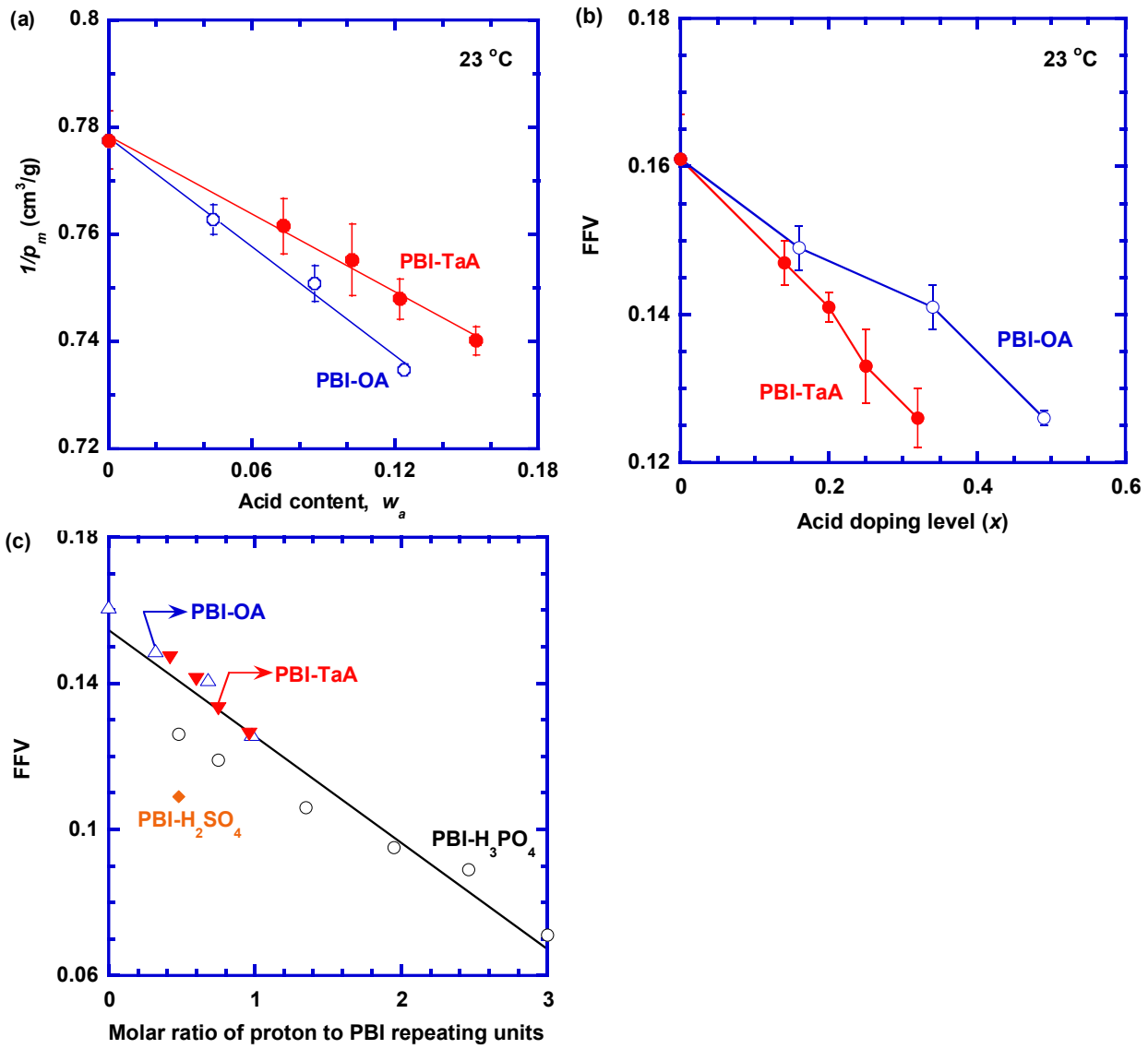

Fig. 3. Effect of the acid doping on ρ_m and *FFV* of the acid-doped PBIs at ≈ 23 °C. (a) Modeling of the density using Eq. (6). (b) *FFV* of PBI-OA and PBI-TaA. (c) Correlation between *FFV* and the molar ratio of the proton to PBI repeating units. The data of PBI-H_3PO_4 and PBI-H_2SO_4 in (c) are from the literature.[4]

The free volume of a polymer is an important parameter to determine its gas diffusivity.[27] However, polymers are often nonporous, and the free volume cannot be directly measured using low-temperature gas adsorption measurement and Brunauer–Emmett–Teller (BET) theory. For example, PBI shows negligible porosity and surface to volume ratio in the BET measurement.[28]

Instead, fractional free volume (*FFV*) of the polymers is often used as an indicator of the free volume and can be estimated from the density using the following equation:[4, 27]

$$FFV = \frac{V - V_0}{V} = \frac{V - 1.3V_w}{V} \quad (7)$$

where V and V_0 are the specific volume and occupied volume, respectively. V_0 equals to 1.3 times of the Van der Waals volume (V_w), which can be estimated by the group contribution method (cf. Table S1). Fig. 3b shows that *FFV* decreases with increasing *x*, which is consistent with the *d*-spacing results and thus confirms the tightened structure by acid doping. The *FFV* of PBI-TaA decreases at a faster rate than that of the PBI-OA because TaA has more carboxylic acid groups and renders a higher cross-linking density than OA. The *FFV* values at 150 ℃ were also estimated and decrease with increasing acid doping level (cf. Fig. S2b).

Fig. 3c displays the correlation between the *FFV* and the molar ratio of the proton to the PBI repeating units in PBI-OA, PBI-TaA, PBI-H_3PO_4, and PBI-H_2SO_4.[4] There seems to be a linear relationship, indicating that the amount of acid groups determines the polymer chains compactness instead of the acidity.

3.2 Effect of the acid doping on gas transport properties

Fig. 4a presents pure-gas H_2 permeability and H_2/CO_2 selectivity at 35 ℃ as a function of the acid doping level. Increasing *x* decreases membrane gas permeability (cf. Fig. S3), which is consistent with the decreased *d*-spacing and *FFV*. H_2/CO_2 selectivity increases dramatically with increasing *x* values due to the increased size-sieving ability, and thus H_2/CO_2 diffusivity selectivity. At the same *x* values, PBI-TaA exhibits higher H_2/CO_2 selectivity than PBI-OA due to the higher

cross-linking density in PBI-TaA. The PBI-TaA$_{0.32}$ exhibits H_2/CO_2 selectivity as high as 45 at 35 °C.

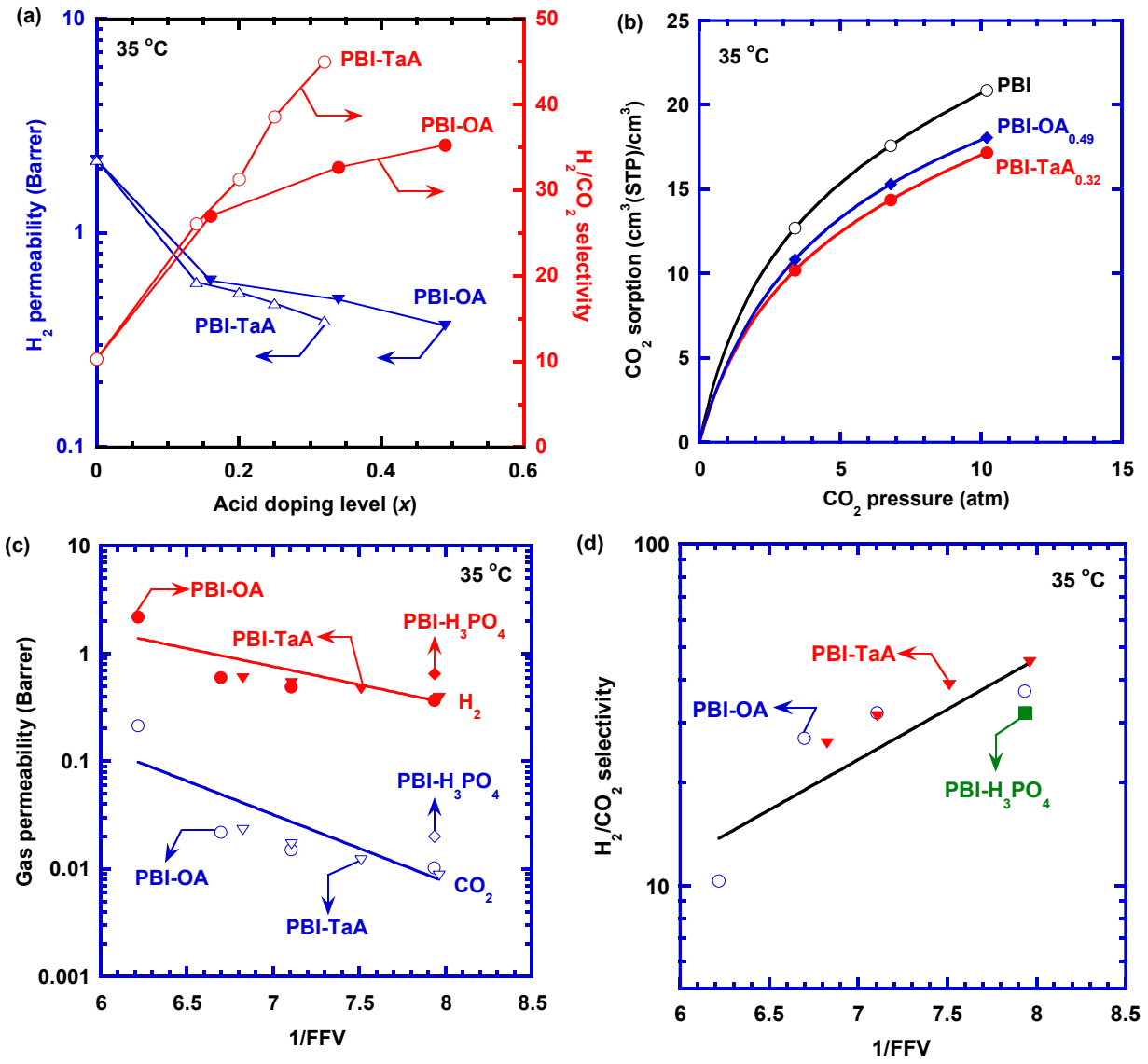

Fig. 4. Pure-gas transport properties in PBI-OA and PBI-TaA at 35 °C. (a) H_2 permeability and H_2/CO_2 selectivity as a function of the acid doping level. (b) CO_2 sorption isotherms. (c) H_2 (filled symbols) and CO_2 (open symbols) permeability and (d) H_2/CO_2 selectivity as a function of $1/FFV$. The curves in (b) are the best fits of the dual-mode sorption model (cf. Eq. 8). The lines in (c) and (d) are the best fits of the free volume model (Eq. 9).

Gas permeability can be decoupled to gas solubility and diffusivity. Fig. 4b compares CO_2

sorption isotherms of PBI, PBI-$OA_{0.49}$, and PBI-$TaA_{0.32}$ at 35 °C. Gas sorption (C_A, $cm^3(STP)/cm^3$) at a constant pressure (p_A, atm) for glassy polymers is often described using the dual-mode sorption model:[29, 30]

$$C_A = k_D p_A + \frac{C_H' b p_A}{1 + b p_A} \tag{8}$$

where k_D is Henry's constant, C_H' is Langmuir sorption capacity, and b is the affinity parameter. The PBI's CO_2 sorption in this study is slightly lower than those reported in the literature, presumably due to the different processing conditions.[4, 7, 31, 32] The sorption isotherms can be satisfactorily described using this model with the values of the adjustable parameters recorded in Table S2.

PBI-$TaA_{0.32}$ and PBI-$OA_{0.49}$ show almost the same CO_2 and C_2H_6 sorption (cf. Fig. 4b and S4), which is slightly lower than PBI due to the lower *FFV* in the doped PBIs. These results suggest that the acid loading or chemical environment has a negligible effect on the gas sorption. By contrast, PBI-$TaA_{0.32}$ and PBI-$OA_{0.49}$ show CO_2 permeability of 0.0087 and 0.0090 Barrer, respectively (cf. Fig. S3). These values are ~95% lower than that of PBI (0.21 Barrer), indicating that the acid doping mainly affects gas diffusivity. Therefore, pure-gas permeability can be correlated with *FFV* using the free volume model:[27]

$$P_A = A_p \exp\left(-\frac{B_p}{FFV}\right) \tag{9}$$

where A_p is a pre-exponential factor, and B_p is a constant that increases with increasing penetrant molecular size.

Fig. 4c shows that both H_2 and CO_2 permeability of PBI-OA, PBI-TaA, and PBI-H_3PO_4 can be fitted with Eq. (9) with a B_p value of 0.90 for H_2 and 1.7 for CO_2. The lower B_p value of H_2 is consistent with its smaller molecular size than CO_2. Fig. 4d shows that the H_2/CO_2 selectivity also correlates well with the free volume model, validating that the gas transport in these samples still follows the solution-diffusion mechanism. Both PBI-$OA_{0.49}$ and PBI-$TaA_{0.32}$ exhibit higher H_2/CO_2 selectivity than PBI-$(H_3PO_4)_{0.16}$ at 35 °C, presumably because of their higher molar ratios of the protons to PBI repeating units and thus higher cross-linking density.

PBI-$OA_{0.49}$ and PBI-$TaA_{0.32}$ were chosen to investigate the effect of temperature on H_2/CO_2 separation properties due to their high H_2/CO_2 selectivity and similar content of the carboxylic acid groups, and the results are shown in Fig. 5a,b. The results for other acid-doped PBIs are reported in Table S3. The pure-gas permeability can be correlated with the temperature using the Arrhenius equation:

$$P_A = P_{A,0} \exp\left(\frac{-E_{P,A}}{RT}\right) \tag{10}$$

where $P_{A,0}$ is a pre-exponential factor, and $E_{P,A}$ is the activation energy for gas permeation. As shown in Fig. 5a, both H_2 and CO_2 permeability can be satisfactorily fitted with the parameters recorded in Table S4. The acid doping of PBI increases the $E_{P,A}$ value due to the increased size-sieving ability. For example, $E_{P,A}$ for H_2 is 24 kJ/mol for PBI, 33 kJ/mol for PBI-$TaA_{0.32}$, and 40 kJ/mol for PBI-$OA_{0.49}$, and $E_{P,A}$ for CO_2 is 24 kJ/mol for PBI, 36 kJ/mol for PBI-$TaA_{0.32}$, and 48 kJ/mol for PBI-$OA_{0.49}$.

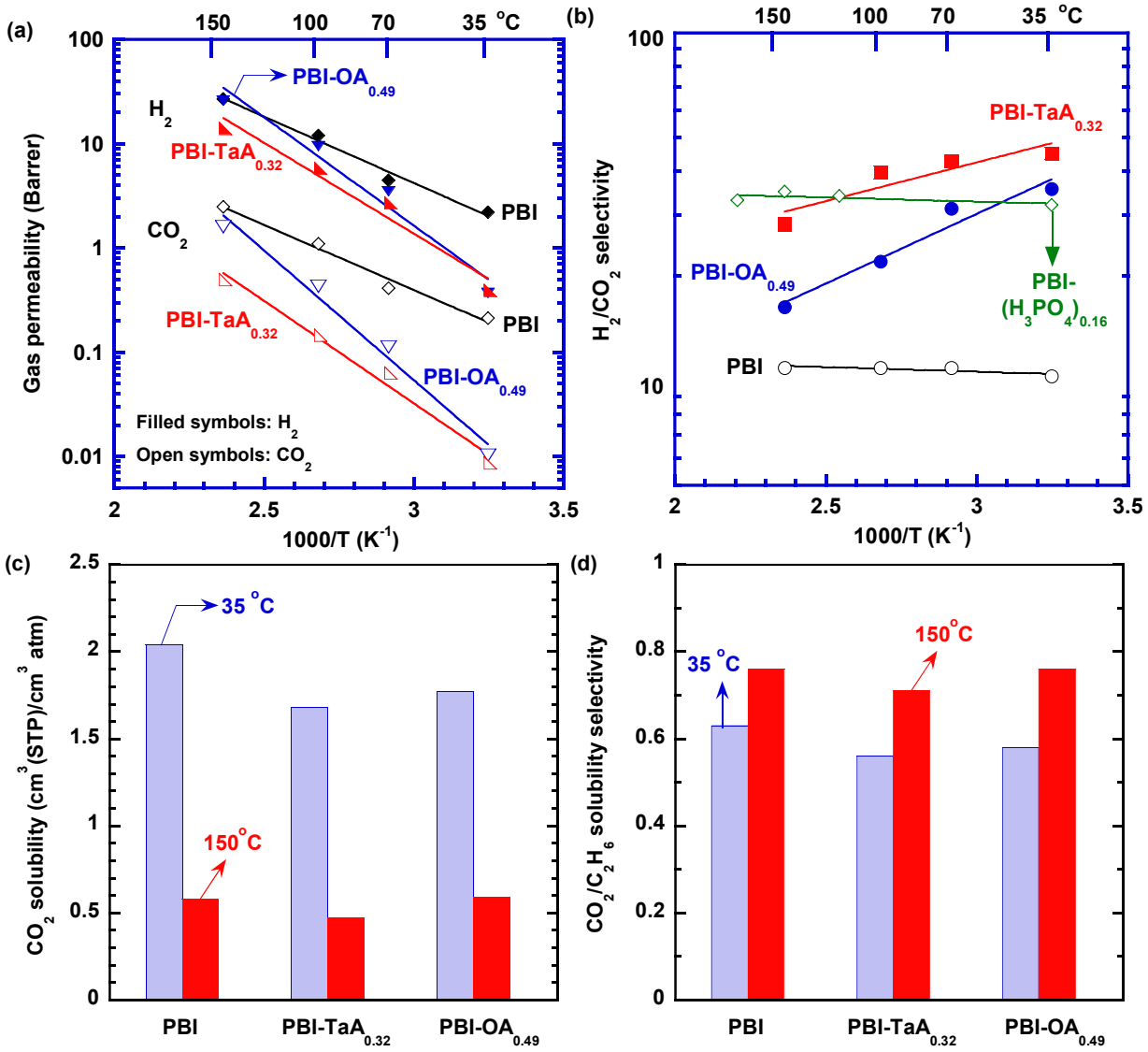

Fig. 5. Effect of temperature on pure-gas transport properties of PBI, PBI-$OA_{0.49}$, and PBI-$TaA_{0.32}$. (a) H_2 and CO_2 permeability; (b) H_2/CO_2 selectivity; (c) CO_2 solubility and (d) CO_2/C_2H_6 solubility selectivity at 10 bar. The lines in (a) and (b) are the best fits of the Arrhenius equation.

Fig. 5b compares the effect of the temperature on pure-gas H_2/CO_2 selectivity for PBI, PBI-$OA_{0.49}$, and PBI-$TaA_{0.32}$. PBI-$TaA_{0.32}$ exhibits the highest H_2/CO_2 selectivity among PBI, PBI-$OA_{0.49}$, and PBI-$TaA_{0.32}$ at all studied temperatures and higher than PBI-$(H_3PO_4)_{0.16}$ at 100 °C and below. Both PBI and PBI-$(H_3PO_4)_{0.16}$ exhibit the selectivity independence of temperature

(consistent with the similar $E_{P,A}$ values for H_2 and CO_2), while the selectivity of PBI-$OA_{0.49}$ and PBI-$TaA_{0.32}$ decreases with increasing temperature (consistent with the lower $E_{P,A}$ values for H_2 than CO_2). For example, H_2/CO_2 selectivity of PBI-$OA_{0.49}$ decreases from 40 to 18 as the temperature increases from 35 °C to 150 °C. The strong size-sieving ability derived from the cross-linking between PBI and OA or TaA appears to be weakened at elevated temperatures, as the hydrogen-bonded –NH becomes free at high temperature.[33-35] By contrast, the unchanged selectivity in PBI and PBI-$(H_3PO_4)_{0.16}$ suggests that the hydrogen bonding between PBI chains or between PBI and H_3PO_4 remains strong up to 200 °C.

Fig. 5c,d presents the effect of temperature on CO_2 and C_2H_6 solubility at 10 bar in PBI, PBI-$TaA_{0.32}$, and PBI-$OA_{0.49}$. H_2 sorption is too low to measure, and C_2H_6 can serve as a surrogate for H_2 since both do not have polar or quadrupole moment to exhibit specific interactions with the polymers.[4, 30, 35, 36] Additionally, CO_2 and C_2H_6 have a similar critical temperature (304.1 K and 305.3 K, respectively), and thus similar condensability. All samples show CO_2/C_2H_6 solubility selectivity less than 1, indicating no specific interaction between CO_2 and the acid-doped PBIs, despite the amine groups of PBI. Increasing the temperature decreases gas solubility (cf. Fig. S4) and slightly increases CO_2/C_2H_6 solubility selectivity. The acid doping slightly decreases the gas solubility and has a negligible effect on CO_2/C_2H_6 solubility selectivity, validating that the acid doping mainly affects gas diffusivity.

3.3 Superior H_2/CO_2 separation performance of the acid-doped PBIs

PBI-$TaA_{0.32}$ shows the highest H_2/CO_2 selectivity among the OA or TaA doped PBIs studied, and therefore, it was selected for further tests with three gas mixtures with H_2:CO_2 molar ratio of

20:80, 50:50, and 80:20 at 7.9 bar and 150 °C. Fig. 6a shows that mixed-gas permeability is independent of CO_2 feed partial pressure and almost the same as the pure-gas permeability, indicating the absence of plasticization due to the low CO_2 sorption at high temperatures.[37] Fig. 6b shows the mixed-gas H_2/CO_2 selectivity of ~30, which is also independent of the CO_2 feed partial pressure.

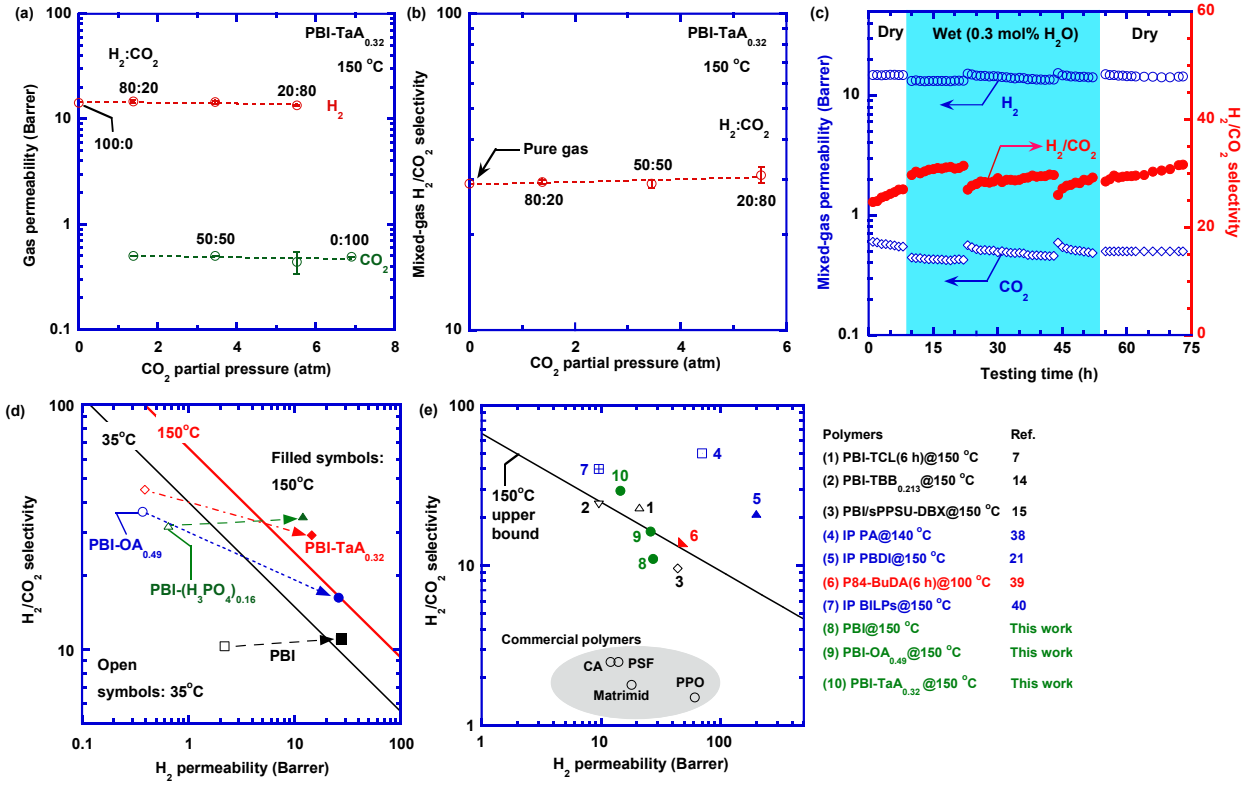

Fig. 6. Superior H_2/CO_2 separation performance of PBI-TaA$_{0.32}$. Effect of the feed CO_2 partial pressure on (a) mixed-gas H_2 and CO_2 permeability and (b) H_2/CO_2 selectivity at 7.9 bar and 150 °C. (c) Long-term stability in dry-wet-dry conditions with H_2/CO_2 of 50:50 at 7.9 bar and 150 °C for 90 h. (d) Pure-gas H_2/CO_2 separation performance of PBI, PBI-OA, PBI-TaA, PBI-$(H_3PO_4)_{0.16}$,[4] and PBI-$(H_2SO_4)_{0.24}$[4] at 35 °C and 150 °C benchmarking with Robeson's 2008 upper bounds. (e) Comparison between the cross-linked PBIs and commercial polymers: PBI-TCL(6 h),[7] PBI-TBB$_{0.213}$,[14] PBI/sPPSU-DBX,[15] IP PA,[38] IP PBDI,[21] P84-BuDA(6 h),[39] and IP BILPs.[40]

Typical coal-derived syngas contains H_2, CO_2, water vapor, and other minor components

(such as H_2S and CO) after the water-gas shift reaction. Fig. 6c presents the effect of water vapor on H_2/CO_2 separation performance and long-term stability at 150 ℃. The sample was first evaluated with a dry gas mixture of 50 % H_2 and 50 % CO_2 for 8 h. Then 0.3 mol% water vapor was introduced, and the test lasted for 43 h before the feed gas was switched back to the dry condition. Although H_2 permeability shows fluctuation with the wet gas, it remains at ~ 15 Barrer, and H_2/CO_2 selectivity remained at ≈ 30. The breaks were caused by the baking of the GC columns to remove residual water, which slightly changed the composition measurement. Both gas permeability and selectivity remain the same after switching back to the dry gas, indicating that PBI-$TaA_{0.32}$ is stable and has the potential for high-temperature H_2/CO_2 separation.

Fig. 6d compares pure-gas H_2/CO_2 separation performance of acid-doped PBIs, including PBI-$OA_{0.49}$, PBI-$TaA_{0.32}$, and PBI-$(H_3PO_4)_x$, at 35 ℃ and 150 ℃ in Robeson's plot.[4, 7, 41] For the acid doped PBIs, the separation performance at 35 ℃ approaches the upper bound. By contrast, at 150 ℃ the acid-doped PBIs exhibit the separation properties above the upper bound. PBI-$TaA_{0.32}$ shows the H_2/CO_2 separation properties similar to the PBI-$(H_3PO_4)_{0.16}$.

Fig. 6e compares H_2/CO_2 separation performance of PBI-$TaA_{0.32}$ and PBI-$OA_{0.49}$ at 150 ℃ with commercial membrane polymers, including polysulfone (PSF),[42] cellulose acetate (CA),[43] Matrimid,[44, 45] and poly(p-phenylene oxide) (PPO).[46] Commercial membrane polymers do not have good H_2/CO_2 selectivity due to the lack of size-sieving ability. Highly cross-linked polyamides (PA) and poly(p-phenylene benzobisimidazole) (PBDI) via interfacial polymerization (IP) show excellent H_2/CO_2 separation performance.[21, 38] Nevertheless, both PBI-$TaA_{0.32}$ and PBI-$OA_{0.49}$ show a good combination of high H_2 permeability and high H_2/CO_2 selectivity.

4. Conclusions

We demonstrate that PBI can be effectively cross-linked by doping with polycarboxylic acids of OA and TaA to improve H_2/CO_2 separation performance at elevated temperatures. The concentration of protons in the PBI films, instead of the acidity strength, plays an important role in influencing the separation properties. Increasing the proton content in PBI decreases the *d*-spacing and *FFV* and thus gas permeability and increases the size-sieving ability and thus H_2/CO_2 selectivity. TaA has more acid groups than OA and is more effective in cross-linking PBI. The acid doping has a negligible effect on gas solubility, and its effect on gas permeability can be satisfactorily described using the free volume model. Increasing the temperature increases gas permeability and slightly decreases H_2/CO_2 selectivity. PBI-$TaA_{0.32}$ exhibits superior and stable H_2/CO_2 separation performance when challenged with wet gas mixtures, which surpasses Robeson's upper bound at 150 ℃, indicating its promise for industrial H_2 purification and CO_2 capture.

ASSOCIATED CONTENT

Supporting Information.

WAXD patterns of PBI and PBI-$OA_{0.49}$ at varied temperatures; *FFV* calculation; pure-gas CO_2 permeability of PBI-OA and PBI-TaA at 35 ℃; parameters of the dual-mode sorption model for CO_2 and C_2H_6 sorption; and activation energy values for H_2 and CO_2 permeation in PBI, PBI-$OA_{0.49}$, and PBI-$TaA_{0.32}$.

AUTHOR INFORMATION

Corresponding Author:

* (H. Lin) Tel: +1-716-645-1856, Email: haiqingl@buffalo.edu.

ORCID

Haiqing Lin: 0000-0001-8042-154X

Notes

The authors declare no competing financial interest.

Author Contributions

The manuscript was written through the contributions of all authors. All authors have given approval to the final version of the manuscript.

ACKNOWLEDGEMENTS

This work was funded by the U.S. Department of Energy (DOE) award No. DE-FE0031636 and the U.S. National Science Foundation (NSF) grant number 1804996. Los Alamos National Laboratory is operated by Triad National Security, LLC for the National Nuclear Security Administration of the U.S. Department of Energy under contract 89233218CNA000001.

REFERENCES

1. Dakhchoune, M.; Villalobos, L. F.; Semino, R.; Liu, L. M.; Rezaei, M.; Schouwink, P.; Avalos, C. E.; Baade, P.; Wood, V.; Han, Y.; Ceriotti, M.; Agrawal, K. V., Gas-Sieving Zeolitic Membranes Fabricated by Condensation of Precursor Nanosheets, *Nat. Mater.* **2020**, in press.
2. Lin, H.; Van Wagner, E.; Freeman, B. D.; Toy, L. G.; Gupta, R. P., Plasticization-Enhanced Hydrogen Purification Using Polymeric Membranes, *Science* **2006,** *311* (5761), 639-642.
3. Merkel, T. C.; Zhou, M. J.; Baker, R. W., Carbon Dioxide Capture with Membranes at an IGCC Power Plant, *J. Membr. Sci.* **2012,** *389*, 441-450.
4. Zhu, L.; Swihart, M.; Lin, H., Unprecedented Size-Sieving Ability in Polybenzimidazole Doped with Polyprotic Acids for Membrane H_2/CO_2 Separation, *Energy Environ. Sci.* **2018,** *11* (1), 94-100.
5. Bui, M.; Adjiman, C. S.; Bardow, A.; Anthony, E. J.; Boston, A.; Brown, S.; Fennell, P. S.; Fuss, S.; Galindo, A.; Hackett, L. A., Carbon Capture and Storage (CCS): The Way Forward, *Energy Environ. Sci* **2018,** *11* (5), 1062-1176.
6. Luo, S.; Zhang, Q.; Zhu, L.; Lin, H.; Kazanowska, B. A.; Doherty, C. M.; Hill, A. J.; Gao, P.; Guo, R., Highly Selective and Permeable Microporous Polymer Membranes for Hydrogen Purification and CO_2 Removal from Natural Gas, *Chem. Mater.* **2018,** *30* (15), 5322-5332.
7. Zhu, L.; Swihart, M.; Lin, H., Tightening Polybenzimidazole (PBI) Nanostructure via Chemical Cross-Linking for Membrane H_2/CO_2 Separation, *J. Mater. Chem. A* **2017,** *5* (37), 19914-19923.
8. Hu, L.; Pal, S.; Nguyen, H.; Bui, V.; Lin, H., Molecularly Engineering Polymeric Membranes for H_2/CO_2 Separation at 100–300 °C, *J. Polym. Sci.* **2020,** *58* (18), 2467-2481.
9. Park, H.; Kamcev, J.; Robeson, L. M.; Elimelech, M.; Freeman, B. D., Maximizing the Right Stuff: The Trade-off Between Membrane Permeability and Selectivity, *Science* **2017,** *356* (6343), eaab0530.
10. Koros, W. J.; Zhang, C., Materials for Next-Generation Molecularly Selective Synthetic Membranes, *Nat. Mater.* **2017,** *16* (3), 289-297.
11. Stevens, K. A.; Moon, J. D.; Borjigin, H.; Liu, R.; Joseph, R. M.; Riffle, J. S.; Freeman, B. D., Influence of Temperature on Gas Transport Properties of Tetraaminodiphenylsulfone (TADPS) Based Polybenzimidazoles, *J. Membr. Sci.* **2020,** *593*, 117427.
12. Singh, R. P.; Li, X.; Dudeck, K. W.; Benicewicz, B. C.; Berchtold, K. A., Polybenzimidazole Based Random Copolymers Containing Hexafluoroisopropylidene Functional Groups for Gas Separations at Elevated Temperatures, *Polymer* **2017,** *119*, 134-141.
13. Zhu, L.; Yin, D.; Qin, Y.; Konda, S.; Zhang, S.; Zhu, A.; Liu, S.; Xu, T.; Swihart, M. T.; Lin, H., Sorption-Enhanced Mixed Matrix Membranes with Facilitated Hydrogen Transport for Hydrogen Purification and CO_2 Capture, *Adv. Funct. Mater.* **2019,** *29* (36), 1904357.
14. Naderi, A.; Tashvigh, A. A.; Chung, T. S., H_2/CO_2 Separation Enhancement via Chemical Modification of Polybenzimidazole Nanostructure, *J. Membr. Sci.* **2019,** *572*, 343-349.
15. Naderi, A.; Chung, T. S.; Weber, M.; Maletzko, C., High Performance Dual-Layer Hollow Fiber Membrane of Sulfonated Polyphenylsulfone/Polybenzimidazole for Hydrogen Purification, *J. Membr. Sci.* **2019,** *591*, 117292.
16. Zhu, L.; Omid, M.; Lin, H., Manipulating Polyimide Nanostructures via Crosslinking for

Membrane Gas Separation. In *Membranes for Gas Separations*, Carreon, M. A., Ed. World Scientific: 2017; Vol. 1, pp 243-270.
17. Gelb, R. I., Conductometric Determination of pKa Values. Oxalic and Squaric Acids, *Anal. Chem.* **1971,** *43* (8), 1110-1113.
18. Pfendt, L.; Drazić, B.; Popović, G.; Drakulić, B.; Vitnik, Z.; Juranić, I., Determination of All pKa Values of Some Di-and Tri-Carboxylic Unsaturated and Epoxy Acids and Their Polylinear Correlation with the Carboxylic Group Atomic Charges, *J. Chem. Res.* **2003,** *2003* (5), 247-248.
19. Qiu, W.; Chen, C.-C.; Kincer, M. R.; Koros, W. J., Thermal analysis and Its Application in Evaluation of Fluorinated Polyimide Membranes for Gas Separation, *Polymer* **2011,** *52* (18), 4073-4082.
20. Chithambaram, V.; Das, S. J.; Krishnan, S.; Ahamed, M. B.; Nambi, R. A., Growth and Characterization of Urea-oxalic Acid Crystals by Solution Growth Technique, *EPJ Appl. Phys.* **2013,** *64* (2), 55-62.
21. Shan, M.; Liu, X.; Wang, X.; Liu, Z.; Iziyi, H.; Ganapathy, S.; Gascon, J.; Kapteijn, F., Novel High Performance Poly(p-Phenylene Benzobisimidazole) (PBDI) Membranes Fabricated by Interfacial Polymerization for H_2 Separation, *J. Mater. Chem. A* **2019,** *7* (15), 8929-8937.
22. Han, S. H.; Lee, J. E.; Lee, K. J.; Park, H. B.; Lee, Y. M., Highly Gas Permeable and Microporous Polybenzimidazole Membrane by Thermal Rearrangement, *J. Membr. Sci.* **2010,** *357* (1-2), 143-151.
23. Hu, L.; Liu, J.; Zhu, L.; Hou, X.; Huang, L.; Lin, H.; Cheng, J., Highly Permeable Mixed Matrix Materials Comprising ZIF-8 Nanoparticles in Rubbery Amorphous Poly(ethylene oxide) for CO_2 Capture, *Sep. Purif. Technol.* **2018,** *205*, 58-65.
24. Huang, L.; Liu, J.; Lin, H., Thermally Stable, Homogeneous Blends of Cross-Linked Poly(ethylene oxide) and Crown Ethers with Enhanced CO_2 Permeability, *J. Membr. Sci.* **2020,** *610*, 118253.
25. Puleo, A. C.; Paul, D. R.; Wong, P. K., Gas Sorption and Transport In Semicrystalline Poly(4-methyl-1-pentene), *Polymer* **1989,** *30* (7), 1357-1366.
26. Golla, M.; Nagendra, B.; Rizzo, P.; Daniel, C.; de Ballesteros, O. R.; Guerra, G., Polymorphism of Poly(2,6-dimethyl-1,4-phenylene)oxide in Axially Stretched Films, *Macromolecules* **2020,** *53* (6), 2287-2294.
27. Park, J.; Paul, D. R., Correlation and Prediction of Gas Permeability in Glassy Polymer Membrane Materials via A Modified Free Volume Based Group Contribution Method, *J. Membr. Sci.* **1997,** *125* (1), 23-39.
28. Omidvar, M.; Nguyen, H.; Huang, L.; Doherty, C. M.; Hill, A. J.; Stafford, C. M.; Feng, X. S.; Swihart, M. T.; Lin, H., Unexpectedly Strong Size-Sieving Ability in Carbonized Polybenzimidazole for Membrane H_2/CO_2 Separation, *ACS Appl. Mater. Interfaces* **2019,** *11* (50), 47365-47372.
29. Maeda, Y.; Paul, D., Effect of Antiplasticization on Gas Sorption and Transport. I. Polysulfone, *J. Polym. Sci., Part B: Polym. Phys.* **1987,** *25* (5), 957-980.
30. Smith, Z. P.; Tiwari, R. R.; Murphy, T. M.; Sanders, D. F.; Gleason, K. L.; Paul, D. R.; Freeman, B. D., Hydrogen Sorption in Polymers for Membrane Applications, *Polymer* **2013,** *54*

(12), 3026-3037.
31. Miller, M. B.; Chen, D.; Luebke, D. R.; Johnson, J. K.; Enick, R. M., Critical Assessment of CO_2 Solubility in Volatile Solvents at 298.15 K, *J. Chem. Eng. Data* **2011,** *56* (4), 1565-1572.
32. Yang, M.; Han, Y.; Zou, E.; Chen, W.; Peng, X.; Dong, B.; Sun, C.; Liu, B.; Chen, G., Separation of IGCC Syngas by Using ZIF-8/Dimethylacetamide Slurry with High CO_2 Sorption Capacity and Sorption Speed but Low Sorption Heat, *Energy* **2020,** *201*, 117605.
33. Skrovanek, D. J.; Howe, S. E.; Painter, P. C.; Coleman, M. M., Hydrogen Bonding in Polymers: Infrared Temperature Studies of an Amorphous Polyamide, *Macromolecules* **1985,** *18* (9), 1676-1683.
34. Moskala, E. J.; Howe, S. E.; Painter, P. C.; Coleman, M. M., On the Role of Intermolecular Hydrogen Bonding in Miscible Polymer Blends, *Macromolecules* **1984,** *17* (9), 1671-1678.
35. Kelman, S.; Lin, H.; Sanders, E. S.; Freeman, B. D., CO_2/C_2H_6 Separation Using Solubility Selective Membranes, *J. Membr. Sci.* **2007,** *305* (1-2), 57-68.
36. Liu, J.; Zhang, S.; Jiang, D.-e.; Doherty, C. M.; Hill, A. J.; Cheng, C.; Park, H. B.; Lin, H., Highly Polar but Amorphous Polymers with Robust Membrane CO2/N2 Separation Performance, *Joule* **2019,** *3* (8), 1881-1894.
37. Coleman, M.; Koros, W., Conditioning of Fluorine-Containing Polyimides. 2. Effect of Conditioning Protocol at 8 Volume Dilation on Gas-Transport Properties, *Macromolecules* **1999,** *32* (9), 3106-3113.
38. Ali, Z.; Pacheco, F.; Litwiller, E.; Wang, Y.; Han, Y.; Pinnau, I., Ultra-Selective Defect-Free Interfacially Polymerized Molecular Sieve Thin-Film Composite Membranes for H_2 Purification, *J. Mater. Chem. A* **2018,** *6* (1), 30-35.
39. Omidvar, M.; Stafford, C. M.; Lin, H., Thermally Stable Cross-Linked P84 with Superior Membrane H_2/CO_2 Separation Properties at 100 ^oC, *J. Membr. Sci.* **2019,** *575*, 118-125.
40. Shan, M.; Liu, X.; Wang, X.; Yarulina, I.; Seoane, B.; Kapteijn, F.; Gascon, J., Facile Manufacture of Porous Organic Framework Membranes for Precombustion CO_2 Capture, *Sci. Adv.* **2018,** *4* (9), eaau1698.
41. Robeson, L. M., The Upper Bound Revisited, *J. Membr. Sci.* **2008,** *320* (1-2), 390-400.
42. Aitken, C. L.; Koros, W. J.; Paul, D. R., Effect of Structural Symmetry on Gas-Transport Properties of Polysulfones, *Macromolecules* **1992,** *25* (13), 3424-3434.
43. Puleo, A. C.; Paul, D. R.; Kelley, S. S., The Effect of Degree of Acetylation on Gas Sorption and Transport Behavior in Cellulose Acetate, *J. Membr. Sci.* **1989,** *47* (3), 301-332.
44. Vu, D.; Koros, W. J.; Miller, S. J., Mixed Matrix Membranes Using Carbon Molecular Sieves - I. Preparation and Experimental Results, *J. Membr. Sci.* **2003,** *211* (2), 311-334.
45. Zhang, Y.; Musseman, I. H.; Ferraris, J. P.; Balkus, K. J., Gas Permeability Properties of Matrimid (R) Membranes Containing the Metal-Organic Framework Cu-BPY-HFS, *J. Membr. Sci.* **2008,** *313* (1-2), 170-181.
46. Koros, W.; Fleming, G.; Jordan, S.; Kim, T.; Hoehn, H., Polymeric Membrane Materials for Solution-Diffusion Based Permeation Separations, *Prog. Polym. Sci.* **1988,** *13* (4), 339-401.

Table of Contents